

Exotic stable calcium carbides

Yan-Ling Li¹, Sheng-Nan Wang², Artem R. Oganov²⁻⁵

Huiyang Gou⁶, Jesse S. Smith⁷, Timothy A. Strobel⁶

1 Laboratory for Quantum Design of Functional Materials, School of Physics and Electronic Engineering, Jiangsu Normal University, 221116, Xuzhou, People's Republic of China

2 Department of Geosciences, State University of New York, Stony Brook, NY 11794-2100, USA

3 Center for Materials by Design, Institute for Advanced Computational Science, State University of New York, Stony Brook, NY 11794-2100, USA

4 Moscow Institute of Physics and Technology, 9 Institutskiy lane, Dolgoprudny city, Moscow Region, 141700, Russian Federation

5 Northwestern Polytechnical University, Xi'an, 710072, People's Republic of China

6 Geophysical Laboratory, Carnegie Institution of Washington, Washington, DC 20015, USA

7 High Pressure Collaborative Access Team, Geophysical Laboratory, Carnegie Institution of Washington, Argonne, Illinois 60439, USA

It is well known that pressure causes profound changes in the properties of atoms and chemical bonding, leading to the formation of many unusual materials. Here we systematically explore all stable calcium carbides at pressures from ambient to 100 GPa using variable-composition evolutionary structure predictions. We find that Ca_5C_2 , Ca_2C , Ca_3C_2 , CaC , Ca_2C_3 , and CaC_2 have stability fields on the phase diagram. Among these, Ca_2C and Ca_2C_3 are successfully synthesized for the first time via high-pressure experiments with excellent structural correspondence to theoretical predictions. Of particular significance are the base-centered monoclinic phase (space group $C2/m$) of Ca_2C , a quasi-two-dimensional metal with layers of negatively charged calcium atoms, and the primitive monoclinic phase (space group $P2_1/c$) of CaC with zigzag C_4 groups. Interestingly, strong interstitial charge localization is found in the structure of $R\text{-}3m\text{-Ca}_5\text{C}_2$ with semimetallic behaviour.

Unexpected chemical reactions can happen under extreme conditions, with emergence of rich phase diagrams and materials possessing intriguing properties. Recently, by combining variable-composition structure prediction methods with first-principles total energy calculations¹, pressure-composition (P - x) phase diagrams were predicted for such binary systems as Mg-O² and Na-Cl³. In both cases, the unexpected compounds that were predicted have been successfully synthesized³ (For the Mg-O system, Goncharov, A. F., personal communication). Elemental carbon and calcium both exhibit rich diversity of stable and metastable phases under pressure⁴⁻⁶. Compressed calcium shows unique structural and electronic properties and exhibits the highest recorded superconducting critical temperature among pure elements⁷. For carbon, only graphite and diamond are experimentally known as thermodynamically stable solids (graphite is thermodynamically stable at ambient condition and diamond under high pressure), although numerous metastable phases are known. For example, by applying pressure to graphite at low temperatures, a new superhard carbon allotrope was found, and its properties match those of one of the theoretically predicted structures (M-carbon)⁸⁻¹¹. For the Ca-C system, the well-known Ca carbides include CaC₂ and CaC₆, whose high-pressure behaviors have been studied experimentally¹²⁻¹⁴ and by *ab initio* calculations¹⁵⁻¹⁹. An interesting structural evolution has been uncovered under pressure: carbon atoms polymerize from dumbbells to 1D-chains to ribbons to 2D graphene sheets in compressed CaC₂¹⁵ and from graphite sheets to a mixed sp^2 - sp^3 structure in CaC₆¹⁹. Also, superconductivity was predicted in metallic high-pressure phases of CaC₂ with critical temperatures

comparable to those observed in CaC_6 ¹⁵.

Here, using variable-composition structure prediction code USPEX^{1,8,20} the pressure-composition phase diagram of the Ca-C system was explored in order to fully understand the structural diversity and evolution of the C-C bonding types under high pressure. This resulted in five newly predicted stable stoichiometries (Ca_5C_2 , Ca_2C , Ca_3C_2 , CaC , and Ca_2C_3) with diverse carbon arrangements: isolated atoms in Ca_2C , hitherto unknown zigzag tetramers in CaC , and ribbons consisting of five-membered rings in CaC_2 . Two phases (Ca_2C and Ca_2C_3) were confirmed experimentally via *in situ* synchrotron powder X-ray diffraction (PXRD) measurements. Most surprising is that the low-pressure phase (monoclinic $C2/m$ structure) of Ca_2C exhibits quasi-two-dimensional metallic behavior and contains negatively charged calcium atoms. Also, strong interstitial electron localization was found in the newly predicted $R-3m$ phase of Ca_5C_2 , just as in compressed elements Li²¹, Na²² and Ca⁵, as well as in the compound Mg_3O_2 ².

Results

Convex hull. We have used the *ab initio* evolutionary algorithm USPEX^{1,8,20}, which can simultaneously find stable stoichiometries and the corresponding structures in multicomponent systems, to explore stable Ca-C compounds and their structures. In these calculations, all stoichiometries were allowed (with the constraint that the total number of atoms in the unit cell be below 16 atoms), and calculations were performed at 10 GPa, 20 GPa, 40 GPa, 80 GPa, and 100 GPa. The pressure-composition phase diagram of the Ca-C system is given in Fig. 1 a, in which the convex hull was

obtained from the calculated enthalpies of the most stable structures for each composition at a given pressure. Thermodynamically, the convex hull at a given pressure connects the phases that are stable against decomposition into other binaries or the elements.

Thermodynamically stable or metastable phases. Using variable-composition evolutionary searches, we found that Ca_5C_2 , Ca_2C , Ca_3C_2 , CaC , Ca_2C_3 , and CaC_2 have thermodynamic stability fields on the phase diagram: Ca_2C_3 , stable from 0 to 28 GPa; Ca_5C_2 , stable above 58 GPa; Ca_2C , stable above 14 GPa; Ca_3C_2 , stable from ~50 GPa; CaC , stable above 26 GPa; and CaC_2 , stable above 21 GPa (see Fig. 1 b and Fig. 2). For all the newly predicted structures, calculated phonon dispersion relations confirmed their dynamical stability. Surprisingly, our theoretical calculations show that the known phases of CaC_2 and CaC_6 are thermodynamically metastable at normal conditions (see Fig. 1 a); CaC_2 is thermodynamically stable only above 21 GPa, and CaC_6 does not have a thermodynamic stability field (BaC_6 is thermodynamically stable in the Ba-C system at 1 atm.²³). We also explored metastable phases of Ca_2C and CaC at lower pressure. The most stable low-pressure phase obtained for Ca_2C has $C2/m$ symmetry and that of CaC has $Immm$ symmetry. The dynamical stability of these two thermodynamically metastable phases was confirmed via phonon calculations.

In order to analyze these predicted structures, we recall that the C-C bond length depends on the bond order and at 1 atm these lengths are 1.20 Å for the triple C-C bond, 1.33 Å for double bond, and 1.54 Å for single C-C bond. The carbon

patterns predicted for calcium carbides, based on calculations presented in this work, are plotted in [Figure 3](#). Combining this knowledge with the results of Bader analysis, we unravel very diverse chemistry. From the results of Bader analysis, one can clearly see the correlation between the charge and volume: negatively charged calcium atoms occupy significantly greater volume. Also we observe the decrease of C-C bond order from triple to double to single bonds as pressure increases. Note, however, that at pressures up to 100 GPa, the most carbon-rich stable compound is CaC_2 . We consider the predicted phases in order of increasing carbon content.

Ca_5C_2 . The stable structure of Ca_5C_2 has $R\bar{3}m$ symmetry. It is a semimetal and is thermodynamically stable at pressures ranging from 58 GPa to at least 100 GPa. This phase has novel structural features: it can be described as consisting of alternating CaC_2 layers (where Ca is octahedrally coordinated by C atoms) and layers with composition Ca_4 . The electron localization function (ELF) distribution in Ca_5C_2 shows strong charge transfer from Ca to C. Non-nuclear charge density maxima are located in the Ca_4 layer as plotted in [Fig. 5](#) (ELF=0.75 at 58 GPa). Bader charges are +1.039 for Ca1, +0.823 for Ca2, +0.973 for Ca3, and -0.459 for the interstitial electron density maximum.

Ca_2C . Known alkali earth methanides include well-known Be_2C ($Fm\bar{3}m$, $Z=4$) and Mg_2C (antifluorite) recently synthesized by Kurakevych *et al.*²⁴. However, no theoretical or experimental information has been reported on the methanide Ca_2C ²⁵. According to our calculations, Ca_2C is thermodynamically stable above 15 GPa (space group $Pnma$ ($Z=4$)). For $Pnma$ - Ca_2C we observe the largest negative charge of

carbon atoms among all these phases: -2.321. In this semiconducting phase with band gap of 0.64 eV at 14 GPa, C atoms are isolated and one can represent this compound as a carbide with an idealized charge transfer scheme $(\text{Ca}^{2+})_2\text{C}^{4-}$ adhering to the Zintl concept. Metallic metastable $C2/m\text{-Ca}_2\text{C}$ has a unique structure, consisting of alternating layers of stoichiometry $\text{Ca}_2(\text{C}_2)$ and Ca_2 (two kinds of calcium atoms play distinctly different roles, see Fig. 6 a), and these layers have net charges of +0.582 and -0.582, respectively. What is unusual is that the Ca-layer is negatively charged, *i.e.*, it is a reservoir of electrons. To further analyze this phenomenon, it is instructive to look first at the $\text{Ca}_2(\text{C}_2)$ layer. This C_2 -group can be represented as having a triple C-C bond and its ideal charge is -2 (Bader charge is -1.892), and if each Ca had the ideal charge of +2, the total charge of the $\text{Ca}_2(\text{C}_2)$ layer would be +2, and two electrons would be transferred to the Ca_2 layer. In reality, the C-C bond here has a somewhat lower order (C-C distance is 1.28 Å at 5 GPa) and therefore takes more electrons from Ca atoms, leaving less for the Ca_2 layer, but not changing the picture qualitatively. ***To our knowledge, this is the first example of negatively charged metal atoms in a compound with more electronegative atoms.*** Note the enormous difference of Bader volumes of the positively and negatively charged Ca atoms (16.570 vs 41.901 Å³). One can expect that the electrons in the Ca-layer are very loosely bound and the work function of this compound can be expected to be extremely low. The density of states of metastable $C2/m$ phase of Ca_2C reveals a remarkable step-like feature near the bottom of the valence band, followed by a nearly constant density of states (see Fig. 6 b), presenting an example of a quasi-two-dimensional electronic structure as observed

in Li-Be alloys²⁶. The calculated Fermi surface of $C2/m$ - Ca_2C at 3 GPa holds a hollow square cylinder-like Fermi surface along the Γ -V direction (*i.e.*, reciprocal lattice basis vector b_3 direction) in the Brillouin zone, signaling quasi-two-dimensional electronic properties (see Fig. 6 c).

Ca₃C₂. For Ca_3C_2 , no thermodynamically stable phase exists below 50 GPa. A metastable $P4/mbm$ ($Z=2$) phase, favored in the pressure range from 5 GPa to 30 GPa, transforms into a $C2/c$ ($Z=4$) structure at 30 GPa, which is thermodynamically stable above 50 GPa. The structure of $P4/mbm$ - Ca_3C_2 contains doubly-bonded C_2 -groups (C-C distance 1.39 Å at 20 GPa), with an ideal charge -4, *i.e.*, accepting four electrons from calcium atoms, leaving two electrons per formula to form Ca-Ca bonds in this metallic compound. Metallic $C2/c$ - Ca_3C_2 with a pseudogap at the Fermi level has singly-bonded C_2 groups (C-C bond length 1.51 Å at 38.7 GPa), which have ideal charge -6, exactly balanced by three Ca atoms in the formula.

CaC. Metallic CaC has two thermodynamically stable phases below 100 GPa. At 14 GPa, the metastable orthorhombic $Immm$ structure transforms into a monoclinic $P2_1/c$ structure (stable thermodynamically above 26 GPa, favored over a wide pressure range of 14-57.5 GPa), followed by a thermodynamic stable $Imma$ structure. $P2_1/c$ -CaC is very interesting because its structural formula $Ca_4(C_4)$ contains a unique and hitherto unknown zigzag C_4 -group, with C-C distances between 1.48-1.50 Å at 14 GPa, indicating bond orders between 1 and 2 and ideal charges of about -2.5 for the end C atoms (Bader charge -1.447) and about -1 for the central C atoms (Bader charge -0.905). $Imma$ -CaC has infinite zigzag chains of C atoms (C-C bond length of

1.55 Å at 57.5 GPa, indicating a weakened single bond) in the y-axis direction. The structural formula of metastable *Immm*-CaC is $\text{Ca}_2(\text{C}_2)$, and with a doubly bonded C_2 -group (C-C distance 1.33 Å at 7.1 GPa) that has an ideal charge of -4 (Bader charge -2.340), it exactly balances the ideal charge of two Ca atoms. All three phases of CaC beautifully conform to the trend of increasing polymerization of the C-sublattice with increasing pressure.

Ca_2C_3 . The structure of Mg_2C_3 (space group *Pnnm*, $Z = 2$), the only known alkaline-earth metal allylenide with C_3^{4-} anions²⁵, was considered when searching for stable phases of Ca_2C_3 . Total energy calculations exclude the possibility of the ambient-pressure Mg_2C_3 -type structure. The semiconducting *C2/m* structure (band gap of 1.06 eV at 10 GPa) is instead the most stable one below 34.5 GPa (thermodynamically stable from 0-28 GPa), followed by metastable *C2/c* structure. By fitting energy vs. volume data to the 3rd-order Birch-Murnaghan equation of state²⁷, the calculated bulk modulus B_0 of *C2/m*- Ca_2C_3 is about 89 GPa, which is higher than that of CaC_2 (50 GPa). At ~40 GPa, the metallic *C2/c* structure transforms into a metastable *P-1* structure (metal), which dominates the pressure range between 40-65 GPa. At higher pressures, a metallic metastable *Imma* structure is stable and contains zigzag carbon chains (Figs. 3 and 4). We searched at much higher pressures for 3D-polymeric carbon frameworks in Ca_2C_3 , but found none at pressures up to at least 300 GPa. For comparison, in CaC_2 we have found that graphene sheets predicted in the high-pressure phase can be stable up to at least 1 TPa¹⁵.

For Ca_2C_3 , the carbon arrangement changes from isolated C_3 to carbon chains to

ribbons (Fig. 3). The structure of $C2/m\text{-Ca}_2\text{C}_3$ can be described as Ca_2 layers linked together by nearly linear symmetric C_3 groups with double C-C bonds (C-C distances 1.32 Å at 18.1 GPa). With this configuration, the total charge of the C_3 group should be -4 (Bader charge -2.692), exactly compensating the charge of two Ca atoms in the formula. Central carbon atoms in the C_3 group in this valence scheme should be neutral, and yet turn out to have the largest negative Bader charge of -0.738, whereas the end atoms, whose idealized charge is -2, develop a lower Bader charge (-0.977). This discrepancy is explained by the effects of Ca atoms, which form significant bonds with the central carbon atom in the C_3 group and transfer some electronic charge to them. Most recently, some of us reported the prediction and synthesis of $\beta\text{-Mg}_2\text{C}_3$ ²⁸, which is isostructural with our $C2/m\text{-Ca}_2\text{C}_3$ reported here. The structure of $C2/c\text{-Ca}_2\text{C}_3$ (C-C distances 1.43-1.47 Å at 34.5 GPa) has an idealized charge transfer scheme $\text{Ca}^{4+}_2\text{C}^{4-}_3$. In this metallic phase, C-atoms are polymerized into infinite chains with nearly closed six-member rings running through channels of Ca host lattice. $P\text{-1-Ca}_2\text{C}_3$ features a complicated extended 1D-ribbon of carbon atoms with nearly single C-C bonds (lengths 1.47-1.50 Å at 40 GPa).

$Imma\text{-Ca}_2\text{C}_3$ has a very interesting structure with extended 1D-ribbons of carbon atoms cut from the graphene layer. Bond lengths in this ribbon are 1.50-1.52 Å at 70 GPa, slightly longer than in graphene and indicating predominantly single bonds. Electronic structure calculations show that both $P\text{-1}$ and $Imma$ phases of Ca_2C_3 are metals. Based on Allen and Dynes modified equation²⁹, we have checked for superconductivity in these phases at 34 GPa and 65 GPa, respectively, and found

none.

CaC₂. CaC₂ is thermodynamically stable above 21 GPa (see Fig. 1 a). The lower pressure phases *C2/m* and *Cmcm* reported previously¹⁵ are metastable, which could be unraveled by calculating enthalpy of formation (ΔH_f) at lower pressure. Considering that graphite is the ground state of carbon at zero pressure, we performed additional calculations where the van der Waals (vdW) interaction is accounted for by using the optPBE-vdW functional³⁰ in our calculation. At zero pressure, the calculated ΔH_f per atom (-0.17 eV) of CaC₂ is close to standard ΔH_f per atom (-0.21 eV at 298K and 1 atm³¹) but higher than that (-0.27 eV) of Ca₂C₃, confirming the thermodynamic metastability of CaC₂ at ambient conditions (see Fig. 1 a). It is very unexpected, but the above numbers fully confirm this conclusion, that the well-known and industrially produced compound CaC₂ is metastable at ambient conditions, while the so far never seen compound Ca₂C₃ is actually stable. This could be either due to kinetics, or due to conditions of synthesis. In addition to our previous result¹⁵, we found a new phase with *P*-1 symmetry, which contains infinite carbon chains with five-membered rings (C-C distance is between 1.442-1.507 Å at 20 GPa (see Fig. 3 i), signaling single or double bonds), and is the lowest enthalpy structure over a wide pressure range from 7.5 GPa to 37 GPa (thermodynamically stable from 21 GPa to 37 GPa, see Fig. 4). With further application of pressure, metallic *P*-1-CaC₂ transforms into metallic *Immm*-CaC₂¹⁵, in which carbon atoms are polymerized to form quasi-one dimensional ribbons (see Figs. 2-3).

Experiments. In order to confirm theoretical structure search predictions, we

performed synthesis studies under high-pressure / high-temperature conditions. Diamond anvil cells were loaded with both calcium- and carbon-rich Ca+C mixtures, compressed to pressures up to 25 GPa, heated to temperatures up to approximately 2000 K and probed *in situ* using synchrotron PXRD. Under these pressure conditions, the formation of *Immm*-CaC₂, *C2/m*-Ca₂C₃ and *Pnma*-Ca₂C may be expected based on thermodynamic stabilities, as these phases are the only stable ones that appear on the convex hull up to 25 GPa (see Fig. 1); indeed, two of these three structures were observed experimentally.

When samples were compressed above ~10 GPa and heated to ~2000 K, mixtures of elemental glassy carbon and face-centered cubic (*fcc*) Ca transformed into a new low-symmetry phase. After comparison with density functional theory (DFT) structure predictions, PXRD reflections originating from this phase were readily indexed to the monoclinic *C2/m*-Ca₂C₃ structure with excellent agreement between experiment and theory. Figure 7 shows experimental PXRD data obtained at 17 GPa with $a = 5.169(4)$ Å, $b = 4.994(3)$ Å, $c = 6.322(3)$ Å and $\beta = 128.53(3)^\circ$ which compares with $a = 5.151$ Å, $b = 4.962$ Å, $c = 6.306$ Å and $\beta = 128.81^\circ$ for calculations relaxed at 18 GPa. This sample was decompressed in steps of ~2 GPa to obtain lattice parameters as a function of pressure (see Fig. 8). Theoretical lattice parameters show an average absolute deviation (AAD) 0.3% from experiment over the entire pressure range, and the *C2/m*-Ca₂C₃ phase was recoverable to ambient pressure, but was found to be air / moisture sensitive. The experimental *P-V* data were fit to a second-order Birch-Murnaghan equation of state with $B_0 = 84(2)$ GPa, in good agreement with

theoretical predictions (89 GPa).

At pressures above ~ 22 GPa, a second carbide phase (*Pnma*-Ca₂C) was synthesized upon laser heating. This same phase was reproducibly formed both from elemental Ca+C mixtures and from samples containing *C2/m*-Ca₂C₃, indicating disproportionation of Ca₂C₃ into a more stable carbide phase above ~ 22 GPa. Figure 7 shows experimental PXRD data at 24 GPa with $a = 6.122(1)$ Å, $b = 4.004(1)$ Å, $c = 7.223(1)$ Å, which compares with $a = 6.044$ Å, $b = 3.977$ Å, $c = 7.265$ Å for DFT calculations at the same pressure. Calculated lattice parameters show an AAD of 0.5% from experimental values between 25-5 GPa (see Fig. 8), which was the lowest pressure obtained due to failure of a diamond anvil. Fitting the P-V data to a second-order Birch-Murnaghan equation of state yields $B_0 = 53(4)$ GPa.

Discussion

We find that the carbon sublattice within all predicted carbide phases has close correlation with the Ca:C ratio (see Fig. 2). With increasing carbon content, isolated carbon atoms are polymerized, in turn, into C₂ dumbbells, C₃ and C₄ groups, chains, ribbons and graphene sheets (see Figs. 4). The polymeric carbon structures reveal an expected trend when comparing to the structural chemistry of the heavier congeners of the 4th main group elements in Zintl phases (alkali or alkaline-earth silicides, germanides, and stannides)^{16, 32}. Yet in spite of certain similarities to silicides, calcium carbides differ from them due to distinct bonding features. Combining present analysis and our previous results^{15,16,19}, one can conclude that for the Ca-C system, one can cover sp to sp^2 to sp^2+sp^3 to sp^3 hybridizations of carbon as pressure

increases. This pressure-induced structural evolution of carbon was also found in other alkali metal or alkaline-earth metal carbides^{16,19,23}. Together with our previous results for CaC_2 ¹⁵ and CaC_6 ¹⁹, it is clear that a three-dimensional network of carbon in CaC_x can be formed when x is greater than 2, (from sheets to three-dimensional frameworks to Ca-C phase separation with slabs of diamond at high C content), consistent also with the behavior of the metastable CaC_4 compound found in our structural searches. On the other hand, the structural features of carbon-rich compounds¹⁹ can be extended to alkali-metal or alkaline-earth metal congeners of the group four elements, which allows one to fabricate a variety of the 3D framework structures of the group four elements by removing metal sublattices. The unexpected mechanical^{19,33} or electronic characteristics³⁴ uncovered in these 3D framework structures pave the way to novel materials.

In summary, we have produced the first complete pressure-composition phase diagram for CaC_x compounds at pressures up to 100 GPa and demonstrated the experimental synthesis of two previously unknown compounds (Ca_2C_3 and Ca_2C), validating part of our predicted phase diagram. Contrary to normal ionic compounds, there is no “dominant” compound stable in this whole pressure range. The well-known CaC_2 and CaC_6 were found to be metastable at normal conditions; CaC_2 is stable only above 21 GPa, and CaC_6 is never thermodynamically stable, while hitherto unreported Ca_2C_3 is actually thermodynamically stable at ambient pressure. Bader analysis unravels very diverse chemistry: the decrease of C-C bond order from triple to double to single bonds at increasing pressure; a negatively charged metal

layer in calcium-rich Ca_2C compound; a hitherto unknown bent linear C_4 group in the $P2_1/c$ phase of CaC ; C-ribbons being present in carbon-rich compounds. The $C2/m$ - Ca_2C phase provides a fresh and very attractive example of a two-dimensional metal, presenting the only known example of a compound where a metal atom (Ca) develops a negative Bader charge in presence of a more electronegative atom (C). Such unusual compounds are likely to find potential applications if synthesized in sufficiently large quantities. While powerful computational methods, such as USPEX, are capable of reliably predicting these exotic compounds, simple theoretical models capable of anticipating them are yet to be developed.

Methods

Structure search and theoretical calculations. Searches for stable structures of the Ca-C system under compression were carried out using the evolutionary algorithm USPEX in combination with the VASP code³⁵ based on density functional theory within the generalized gradient approximation with the exchange-correlation functional of Perdew, Burke and Ernzerhof³⁶, employing the projector augmented-wave (PAW)³⁷ method where $2s^22p^2$ and $3s^23p^64s^2$ are treated as valence electrons for C and Ca atoms, respectively. For carbon, a ‘hard’ pseudopotential was used in searching for stable structures. For the crystal structure searches, we used a plane-wave basis set cutoff of 700 eV and performed the Brillouin zone integrations using a coarse k-point grid. The most interesting structures were further relaxed at a higher level of accuracy with a basis set cutoff of 1000 eV and a k-point grid of spacing $2\pi \times 0.018 \text{ \AA}^{-1}$. Iterative relaxation of atomic positions was stopped when all forces were smaller than $0.001 \text{ eV \AA}^{-1}$. For compounds predicted via variable-composition searches, we re-searched their stable structures using fixed-composition calculations, with two, three, and four formula units per unit cell. For Ca_2C_3 , some evolutionary calculations were also performed under the pressure of 30 GPa, 50 GPa, 80 GPa, 120 GPa, 160 GPa, 240 GPa, and 300 GPa with two or four chemical formula units per unit cell so as to discern the possibility of three-dimensional network carbon.

The enthalpy of formation per atom of Ca_nC_m is defined as $\Delta H_f(\text{Ca}_n\text{C}_m) = [\text{H}(\text{Ca}_n\text{C}_m) - n\text{H}(\text{Ca}) - m\text{H}(\text{C})]/(n+m)$, where all enthalpies H are given at

the same pressure and zero temperature. At a given pressure, the calcium carbides located on the convex hull are thermodynamically stable against decomposition to any other binaries or the elements while the compound above the convex hull meta-stable.

Bader analysis was performed for exploring chemical bonding and local electrons³⁸. To get a converged charge density, the plane wave kinetic energy cutoff of 1000 eV and Monkhorst-Pack **k**-point meshes with the reciprocal space resolution of $2\pi \times 0.02 \text{ \AA}^{-1}$ were used for all the structures. A series of FFT grids to accurately reproduce the correct total core charge were tested by increasing parameters NG(X,Y,Z)F to 1.5, 2 and 2.5 times the default one.

The lattice dynamics and superconducting properties of Ca_2C_3 were calculated by the Quantum ESPRESSO package³⁹ using Vanderbilt-type ultrasoft pseudopotentials with cutoff energies of 50 Ry and 500 Ry for the wave functions and the charge density, respectively. The electronic Brillouin zone (BZ) integration in the phonon calculation was based on a $12 \times 12 \times 12$ of Monkhorst-Pack **k**-point meshes. The dynamic matrix was computed based on a $6 \times 6 \times 6$ mesh of phonon wave vectors. The electron-phonon coupling was convergent with a finer grid of $48 \times 48 \times 48$ **k** points and a Gaussian smearing of 0.01 Ry. For other compounds, phonon calculations were performed using the Phonopy code⁴⁰. The Fermi surface of $\text{C2}/m\text{-Ca}_2\text{C}$ at 3 GPa was calculated via Quantum Espresso code using Vanderbilt-type ultrasoft pseudopotentials with $16 \times 16 \times 8$ of Monkhorst-Pack **k**-point meshes.

Experiment. Reagents for experimental studies consisted of commercial

calcium metal (Sigma-Aldrich, dendritic pieces, 99.99%) and glassy carbon (Sigma-Aldrich, 2-12 μm , 99.95%). The carbon powder was degasified for 12 hours at $\sim 200^\circ\text{C}$ in a vacuum oven and then sealed under Ar. Diamond anvil cell syntheses (up to 25 GPa and 2000 K with *in situ* PXRD) were performed at HPCAT, sector 16, of the Advanced photon Source. A small amount of carbon powder and Ca metal shavings were pressed in thin layers within a rhenium gasket in a diamond anvil cell equipped with 400- μm culet diamonds inside of an inert Ar glovebox ($\text{O}_2 < 1 \text{ ppm}$; $\text{H}_2\text{O} < 1 \text{ ppm}$). It was not possible to control the precise Ca:C ratio, but compositions were estimated to range between $0.333 \leq \text{Ca:C} \leq 3$, based upon the volume of material loaded into the diamond cell. Samples were sealed inside the glovebox without pressure medium or loaded with Ne to improve thermal isolation from diamonds and quasi-hydrostatic conditions for subsequent diffraction measurements. Pressure was estimated using the Ne equation of state⁴¹ and/or with a ruby gauge⁴². To generate high temperatures, samples were heated on both sides using IR fiber lasers. In some cases two or three heating cycles were performed, with X-ray diffraction patterns collected before, during, and after laser heating. During laser heating, temperatures from each side of the sample were estimated by collecting emitted thermal radiation, correcting for the optical system response and fitting the spectral data to Planck's equation. Angle-dispersive PXRD patterns were collected using a MAR image plate calibrated with a CeO_2 standard. Patterns were integrated using FIT2D⁴³ and phase recognition and indexing were performed using PowderCell and CheckCell programs⁴⁴. While observed PXRD intensities were in good agreement

with DFT-derived structural models, observed powder statistics were not suitable for Rietveld refinements. Full profile refinements were performed using the Le Bail intensity extraction method, as implemented in GSAS⁴⁵ with EXPGUI⁴⁶.

References

- 1 Lyakhov, A. O., Oganov, A. R., Stokes, H. T. & Zhu, Q. New developments in evolutionary structure prediction algorithm USPEX. *Comput. Phys. Commun.* **184**, 1172-1182 (2013).
- 2 Zhu, Q., Oganov, A. R. & Lyakhov, A. O. Novel stable compounds in the Mg-O system under high pressure. *Phys. Chem. Chem. Phys.* **15**, 7696-7700 (2013).
- 3 Zhang, W. *et al.* Unexpected stable stoichiometries of sodium chlorides. *Science* **342**, 1502-1505 (2013).
- 4 Zhu, Q., Zeng, Q. & Oganov, A. R. Systematic search for low-enthalpy sp^3 carbon allotropes using evolutionary metadynamics. *Phys. Rev. B* **85**, 201407 (2012).
- 5 Oganov, A. R. *et al.* Exotic behavior and crystal structures of calcium under pressure. *P. Natl. Acad. Sci. USA*. **107**, 7646-7651 (2010).
- 6 Fujihisa, H. *et al.* Ca-VII: A chain ordered host-guest structure of calcium above 210 GPa. *Phys. Rev. Lett.* **110**, 235501 (2013).
- 7 Sakata, M., Nakamoto, Y., Shimizu, K., Matsuoka, T. & Ohishi, Y. Superconducting state of Ca-VII below a critical temperature of 29 K at a pressure of 216 GPa. *Phys. Rev. B* **83**, 220512 (2011).
- 8 Oganov, A. R. & Glass, C. W. Crystal structure prediction using ab initio evolutionary techniques: Principles and applications. *J. Chem. Phys.* **124**, 244704-244715 (2006).
- 9 Li, Q. *et al.* Superhard monoclinic polymorph of carbon. *Phys. Rev. Lett.* **102**, 175506-175504 (2009).
- 10 Boulfelfel, S. E., Oganov, A. R. & Leoni, S. Understanding the nature of “superhard graphite”. *Sci. Rep.* **2**, 471 (2012).
- 11 Wang, Y., Panzik, J. E., Kiefer, B. & Lee, K. K. M. Crystal structure of graphite under room-temperature compression and decompression. *Sci. Rep.* **2**, 520 (2012).
- 12 Nysten, J., Konar, S., Lazor, P., Benson, D. & Haussermann, U. Structural behavior of the acetylide carbides Li_2C_2 and CaC_2 at high pressure. *J. Chem. Phys.* **137**, 224507-224508 (2012).
- 13 Gauzzi, A. *et al.* Enhancement of superconductivity and evidence of structural instability in intercalated graphite CaC_6 under high pressure. *Phys. Rev. Lett.* **98**, 067002-067004 (2007).
- 14 Debessai, M. *et al.* Superconductivity for CaC_6 to 32 GPa hydrostatic pressure. *Phys. Rev. B* **82**, 132502 (2010).
- 15 Li, Y.-L. *et al.* Pressure-induced superconductivity in CaC_2 . *P. Natl. Acad. Sci. USA*. **110**, 9289-9294 (2013).
- 16 Benson, D. *et al.* Lithium and calcium carbides with polymeric carbon structures. *Inorg. Chem.* **52**, 6402-6406 (2013).
- 17 Zhang, L. *et al.* Pressure-induced enhancement of electron-phonon coupling in superconducting CaC_6 from first principles. *Phys. Rev. B* **74**, 184519 (2006).
- 18 Csányi, G., Pickard, C. J., Simons, B. D. & Needs, R. J. Graphite intercalation compounds under pressure: a first-principles density functional theory study. *Phys. Rev. B* **75**, 085432 (2007).
- 19 Li, Y. -L. *et al.* Formation of nanofoam carbon and re-emergence of superconductivity in compressed CaC_6 . *Sci. Rep.* **3**, 3331 (2013).
- 20 Oganov, A. R., Lyakhov, A. O. & Valle, M. How evolutionary crystal structure prediction

- works—and why. *Acc. Chem. Res.* **44**, 227-237 (2011).
- 21 Pickard, C. J. & Needs, R. J. Dense low-coordination phases of lithium. *Phys. Rev. Lett.* **102**, 146401-146404 (2009).
 - 22 Ma, Y. *et al.* Transparent dense sodium. *Nature* **458**, 182-185 (2009).
 - 23 Wang, D.-H. *et al.* BaC: a thermodynamically stable layered superconductor. *Phys. Chem. Chem. Phys.* **16**, 20780-20784 (2014).
 - 24 Kurakevych, O. O., Strobel, T. A., Kim, D. Y. & Cody, G. D. Synthesis of Mg₂C: a magnesium methanide. *Angew. Chem. Int. Ed.* **52**, 8930-8933 (2013).
 - 25 Ruschewitz, U. Binary and ternary carbides of alkali and alkaline-earth metals. *Coord. Chem. Rev.* **244**, 115-136 (2003).
 - 26 Feng, J., Hennig, R. G., Ashcroft, N. W. & Hoffmann, R. Emergent reduction of electronic state dimensionality in dense ordered Li-Be alloys. *Nature* **451**, 445-448 (2008).
 - 27 Birch, F. Finite Elastic Strain of Cubic Crystals. *Phys. Rev.* **71**, 809-824 (1947).
 - 28 Timothy, A. S. *et al.* Synthesis of β -Mg₂C₃: a monoclinic high-pressure polymorph of magnesium sesquicarbide. *Inorg. Chem.* **53**, 7020-7027 (2014).
 - 29 Allen, P. B. & Dynes, R. C. Transition temperature of strong-coupled superconductors reanalyzed. *Phys. Rev. B* **12**, 905-922 (1975).
 - 30 Klimeš, J., Bowler, D. R., & Michaelides, A. Van der Waals density functionals applied to solids. *Phys. Rev. B* **83**, 195131 (2011).
 - 31 Standard enthalpy change of formation. <http://en.wikipedia.org/wiki/> (2014).
 - 32 Gao, G., Ashcroft, N. W., Miao, M., & Hoffmann, R. Novel Si networks in the Ca/Si phase diagram under pressure. *J. Phys. Chem. C* **118**, 25167-25175 (2014).
 - 33 Jiang, X., Zhao, J., Li, Y. L. & Ahuja, R.. Tenable assembly of sp³ cross-linked 3D graphene monoliths: A first-principles prediction. *Adv. Funct. Mater.* **23**, 5846-5853 (2013).
 - 34 Kim, D. Y., Stefanoski, S., Kurakevych, O. O. & Strobel, T. A. Synthesis of an open-framework allotrope of silicon. *Nat. Mater.* **14**, 169-173 (2015).
 - 35 Hafner, J. Materials simulations using VASP—a quantum perspective to materials science. *Comput. Phys. Commun.* **177**, 6-13 (2007).
 - 36 Perdew, J. P., Burke, K. & Ernzerhof, M. Generalized gradient approximation made simple. *Phys. Rev. Lett.* **77**, 3865-3868 (1996).
 - 37 Kresse, G. & Joubert, D. From ultrasoft pseudopotentials to the projector augmented-wave method. *Phys. Rev. B* **59**, 1758-1775 (1999).
 - 38 Henkelman, G., Arnaldsson, A. & Jónsson, H. A fast and robust algorithm for Bader decomposition of charge density. *Comp. Mater. Sci.* **36**, 354-360 (2006).
 - 39 Giannozzi, P. *et al.* QUANTUM ESPRESSO: a modular and open-source software project for quantum simulations of materials. *J. Phys: condens. Mat.* **21**, 395502 (2009).
 - 40 Togo, A., Oba, F. & Tanaka, I. First-principles calculations of the ferroelastic transition between rutile-type and CaCl₂-type SiO₂ at high pressures. *Phys. Rev. B* **78**, 134106 (2008).
 - 41 Hemley, R. J. *et al.* X-ray diffraction and equation of state of solid neon to 110 GPa. *Phys. Rev. B* **39**, 11820-11827 (1989).
 - 42 Mao, H. K., Xu, J. & Bell, P. M. Calibration of the ruby pressure gauge to 800 kbar under quasi-hydrostatic conditions. *J. Geophys. Res.: Solid Earth* **91**, 4673-4676 (1986).
 - 43 Hammersley, A. P. FIT2D: an introduction and overview. *ESRF Internal Report ESRF97HA02T* (1997).

- 44 LMGP-suite suite of programs for the interpretation of X-ray experiments, by Jean Laugier
and Bernard Bochu, ENSP/Laboratoire des Matériaux et du Génie Physique, BP 46. 38042
Saint Martin d'Hères, France.
- 45 Larson, A. C. & Von Dreele, R. B. Los Alamos National Laboratory Report LAUR. 86-748
(1994).
- 46 Toby, B. H. EXPGUI, a graphical user interface for GSAS. *J. Appl. Crystallogr.* **34**, 210-213
(2001).

Acknowledgements

Y.L.L acknowledges support from the NSFC (11347007), Qing Lan Project, and the Priority Academic Program Development of Jiangsu Higher Education Institutions (PAPD). A.R.O and S.N.W thank the National Science Foundation (EAR-1114313, DMR-1231586), DARPA (Grants No. W31P4Q1210008 and No. W31P4Q1310005), the Government of Russian Federation (No. 14.A12.31.0003) for financial support, and Foreign Talents Introduction and Academic Exchange Program (No. B08040). Calculations were performed on XSEDE facilities and on the cluster of the Center for Functional Nanomaterials, Brookhaven National Laboratory, which is supported by the DOE-BES under contract no. DE-AC02-98CH10086. Experimental efforts were supported by DARPA under grant No. W31P4Q1310005. Portions of this work were performed at HPCAT (Sector 16), Advanced Photon Source (APS), Argonne National Laboratory. HPCAT operations are supported by DOE-NNSA under Award No. DE-NA0001974 and DOE-BES under Award No. DE-FG02-99ER45775, with partial instrumentation funding by NSF. The Advanced Photon Source is a U.S. Department of Energy (DOE) Office of Science User Facility operated for the DOE Office of Science by Argonne National Laboratory under Contract No. DE-AC02-06CH11357.

Author contributions

Y.L.L and A.R.O designed the research. Y.L.L, A.R.O, and S.N.W performed calculations. H.G, J.S.S and T.A.S performed the experimental studies. All authors analyzed the data and contributed to write the paper.

Figure legends

Figure 1. Stability of new calcium carbides. (a) Convex hull diagram for the Ca-C system at selected pressures. At a given pressure, the compounds located on the convex hull are thermodynamic stable. (b) Pressure-composition phase diagram of the Ca-C system. Thick solid lines represent thermodynamically stable phases and dashed lines represent metastable phases (Red lines represent metal and blue semiconductor.).

Figure 2. The predicted crystal structures of stable Ca-C compounds. (a) Thermodynamically stable *Pnma* structure of Ca_2C . (b) The metastable low pressure *P4/mbm* structure of Ca_3C_2 . (c) Thermodynamically stable high pressure *C2/c* structure of Ca_3C_2 . (d) Thermodynamically stable *P2₁/c* structure of CaC . (e) Thermodynamically stable high pressure *Imma* structure of CaC . (f) Ca_2C_3 crystallizes in *C2/m* structure at pressures up to 28 GPa. (g) Thermodynamically metastable *C2/c* structure of Ca_2C_3 . (h) Thermodynamically metastable *P-1* structure of Ca_2C_3 . (i) Thermodynamically metastable high pressure *Imma* of Ca_2C_3 . (j) Thermodynamically stable *P-1* structure of CaC_2 . (k) Thermodynamically stable *Immm* structure of CaC_2 . The blue and brown spheres represent calcium and carbon atoms, respectively.

Figure 3. Carbon patterns in the Ca-C system. (a) The isolated carbon anions in the *Pnma* structure of Ca_2C . (b) Cdimers observed in the *C2/m* structure of Ca_2C , *P4/mbm* and *C2/c* structures of Ca_3C_2 , *Imma* structure of CaC , *C2/c* structures of Ca_2C_3 , and *C2/m* or *C2/c* structures of CaC_2 . (c) The carbon trimer occurs in the *C2/m* structure of Ca_2C_3 at zero pressure. (d) Zigzag C_4 groups observed in *P2₁/c* structure of CaC at 20 GPa. (e) Zigzag carbon chains in the *Imma* structure of CaC at 58 GPa. (f) Carbon chains with two types of carbon-carbon bondings in *C2/c* structure of Ca_2C_3 at 34.5 GPa. (g) Carbon chains with four types of carbon-carbon bondings in *P-1* structure of Ca_2C_3 at 40 GPa. (h) Armchair carbon chains in the *Cmcm* structure of CaC_2 at 4 GPa. (i) Carbon stripes in the *P-1* structure of CaC_2 at 20 GPa. (j) Carbon ribbons in the *Immm* structure of CaC_2 at 10 GPa. (k) Carbon ribbons in the *Imma* structure of Ca_2C_3 at 65 GPa. Bond lengths (in Å) are given. The inequivalent

C1, C2, C3, and C4 (occupying different Wyckoff positions in the unit cell) are shown by red, blue, yellow, and grey spheres, respectively.

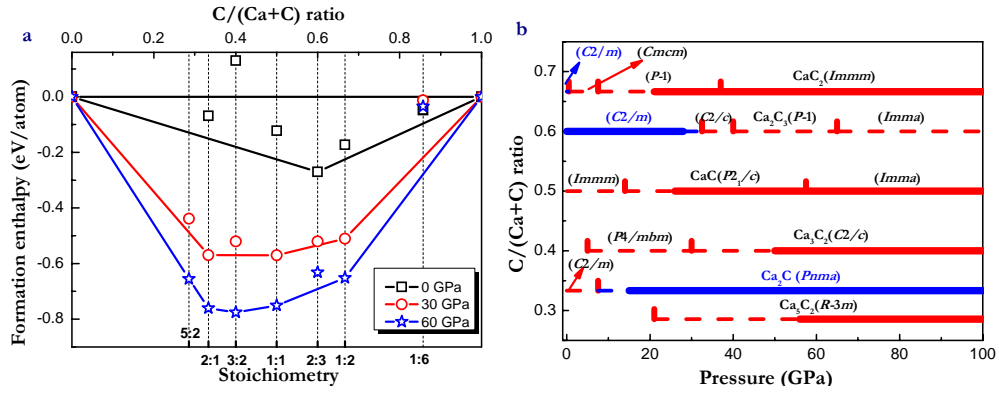
Figure 4. Carbon arrangement with increasing carbon content. Only thermodynamically stable phases are shown. Additionally, the conducting properties are shown.

Figure 5. Electron localization function (ELF) of $R\text{-}3m\text{-Ca}_5\text{C}_2$ at 60 GPa. The isosurface $\text{ELF}=0.75$ is shown. The observed interstitial electron charge accumulation shows that Ca_5C_2 with $R\text{-}3m$ symmetry is an electride.

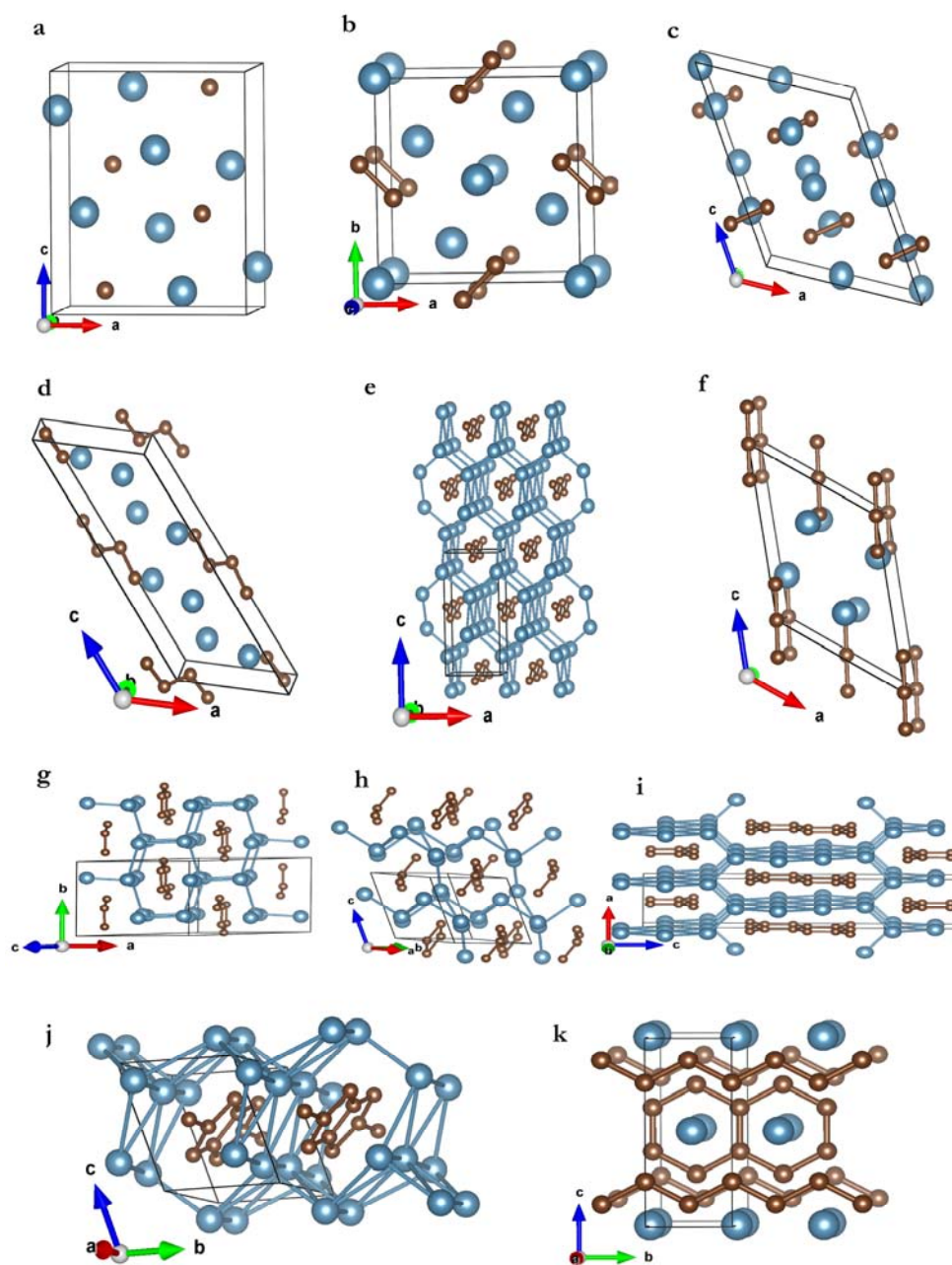
Figure 6. Structural and electronic property of $C2/m$ phase of Ca_2C at 3 GPa. (a) The top view of $C2/m$ structure along the y axis shows a clearly layered structure. (b) Total electronic density of states (DOS). (c) Fermi surface of the $C2/m$ structure. The indication of a quasi-two-dimensional metal in total DOS is confirmed by the hollow square prismatic cylinder-like Fermi surface.

Figure 7. PXRD patterns for experimentally observed Ca-C phases. (a) $Pnma\text{-Ca}_2\text{C}$ synthesized at 24 GPa ($wR_p = 1.5\%$, $R_p = 0.9\%$). (b) $C2/m\text{-Ca}_2\text{C}_3$ synthesized at 17 GPa ($wR_p = 2.0\%$, $R_p = 0.9\%$). Experimental data (points) are compared with full-profile refinements using the Le Bail method (blue lines), with differences (red lines). Simulated powder patterns using atomic positions derived from DFT-optimized structures are shown for intensity comparison (green lines). Positions of reflections of Ca_2C (a) or Ca_2C_3 (b), Ca, Ne and a third carbide phase are indicated by black, green, blue and red tick marks, respectively.

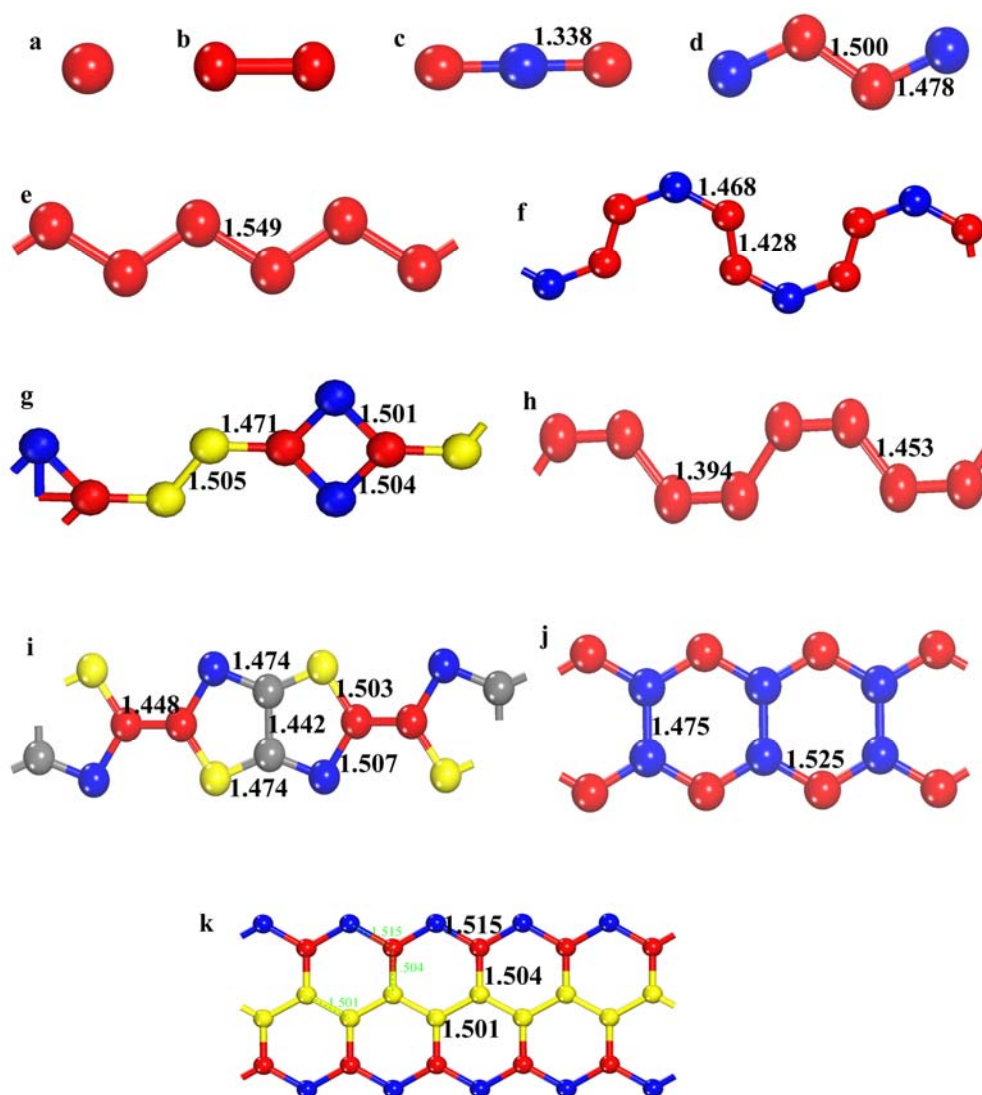
Figure 8. Lattice parameters and unit cell volumes for Ca-C phases. Experimental parameters (points) are compared with DFT predictions (dashed lines) for both $C2/m\text{-Ca}_2\text{C}_3$ (a) and $Pnma\text{-Ca}_2\text{C}$ (b). Experimentally-derived equations of state for both phases are shown as solid lines in the lower panels.



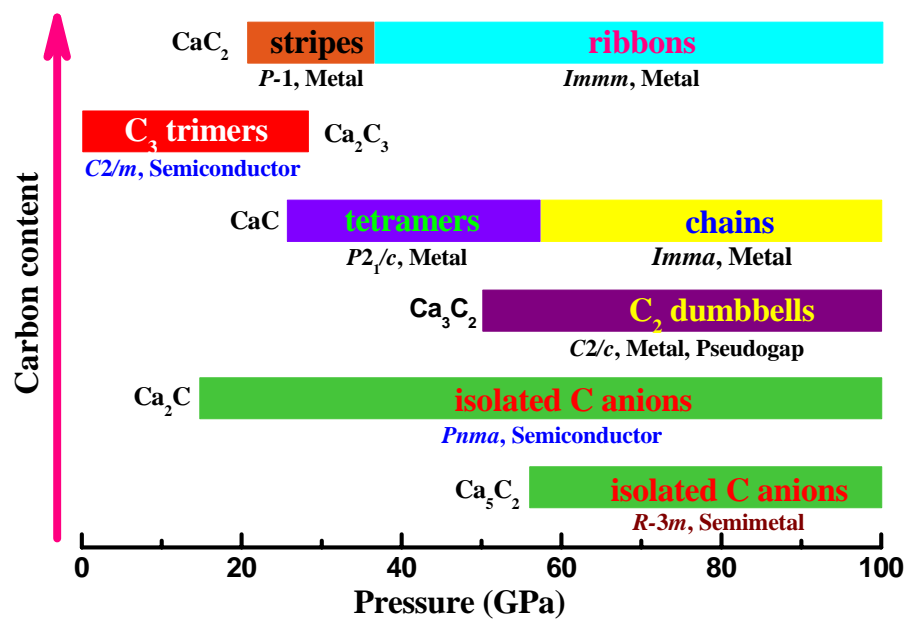
Li *et al.* Fig. 1.



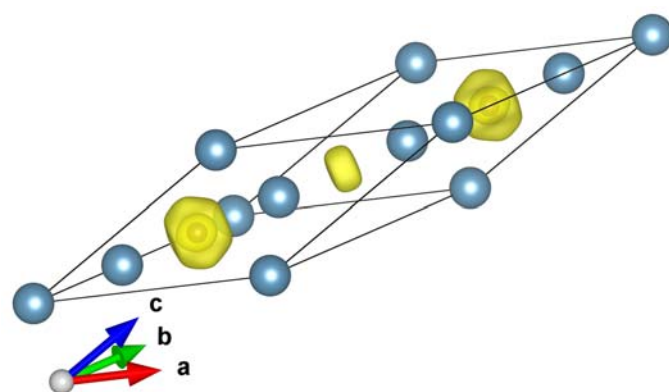
Li *et al.* Fig. 2.



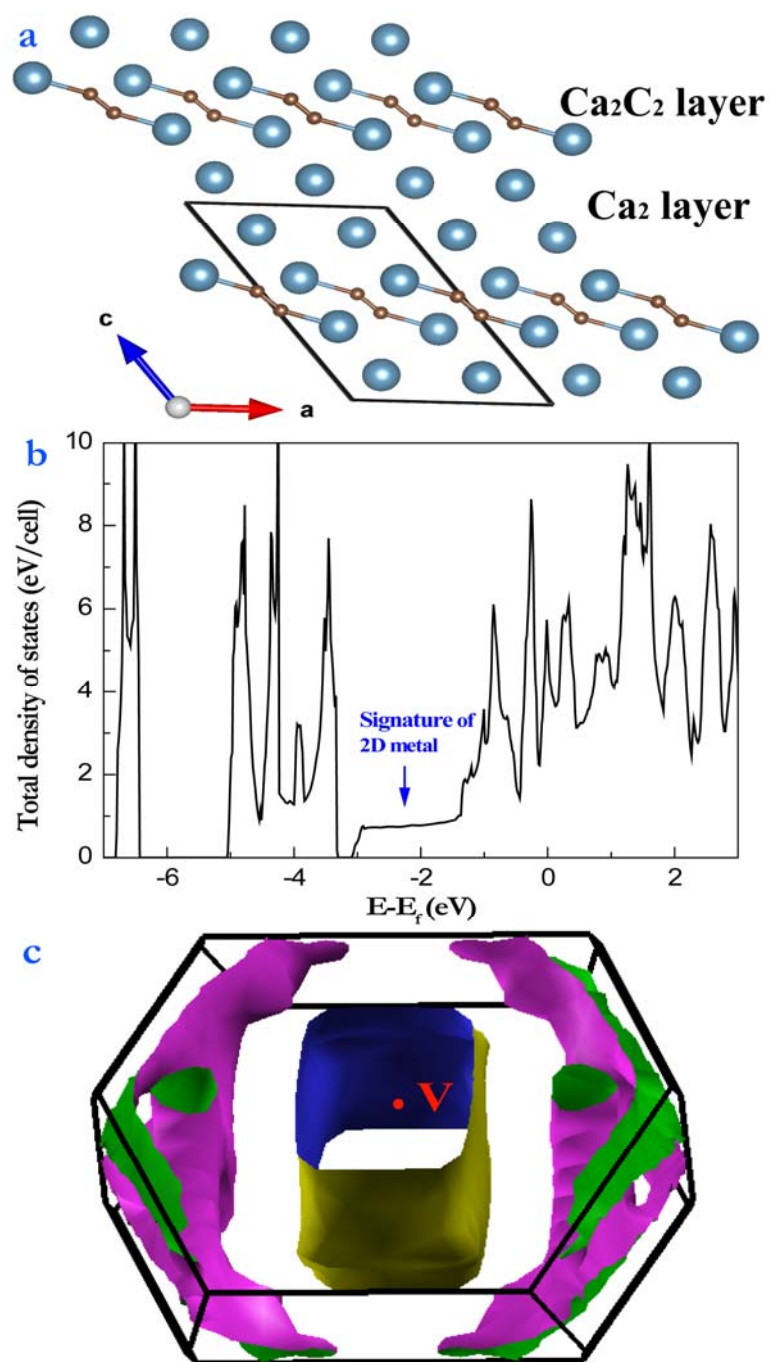
Li *et al.* Fig. 3.



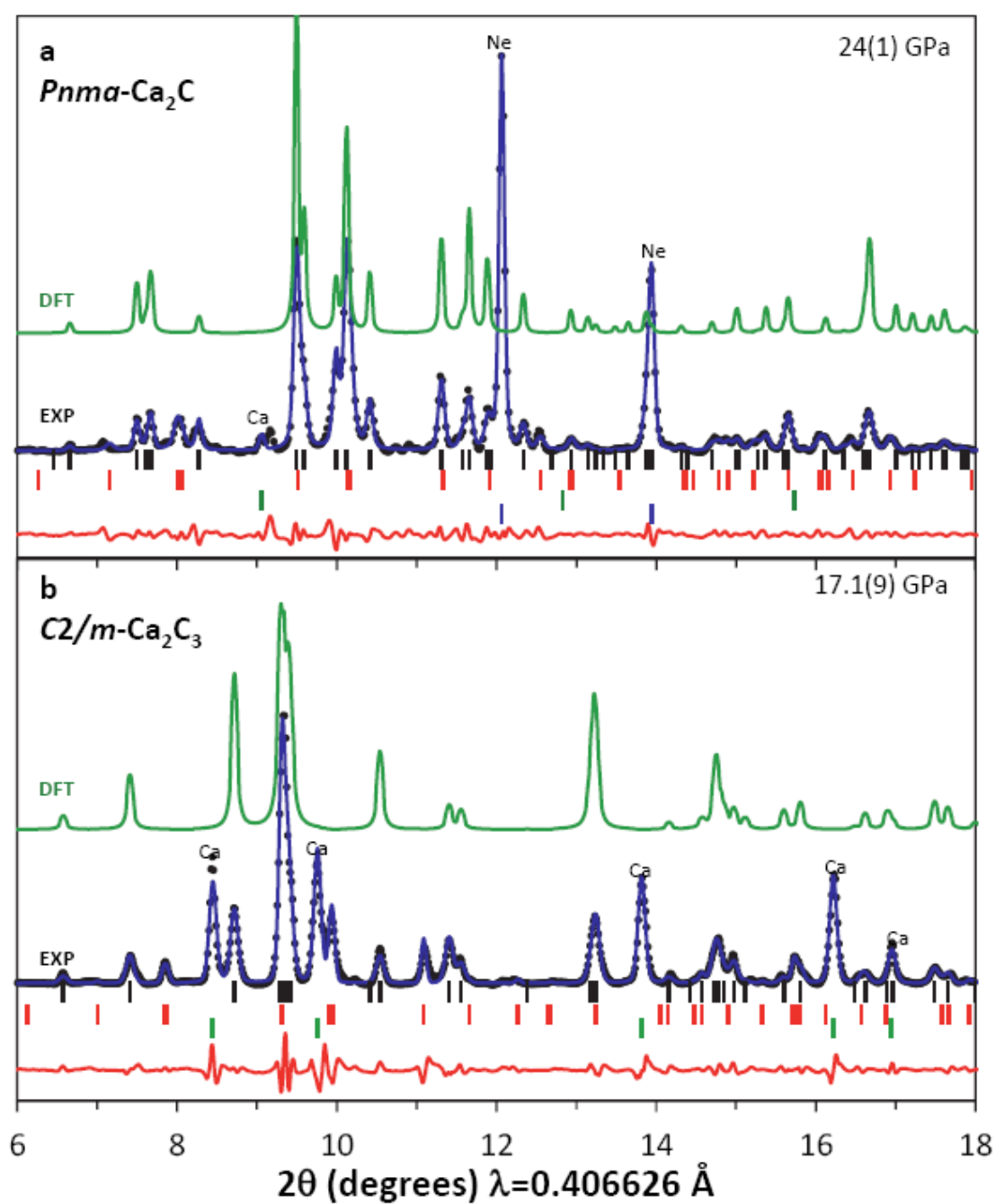
Li *et al.* Fig. 4.



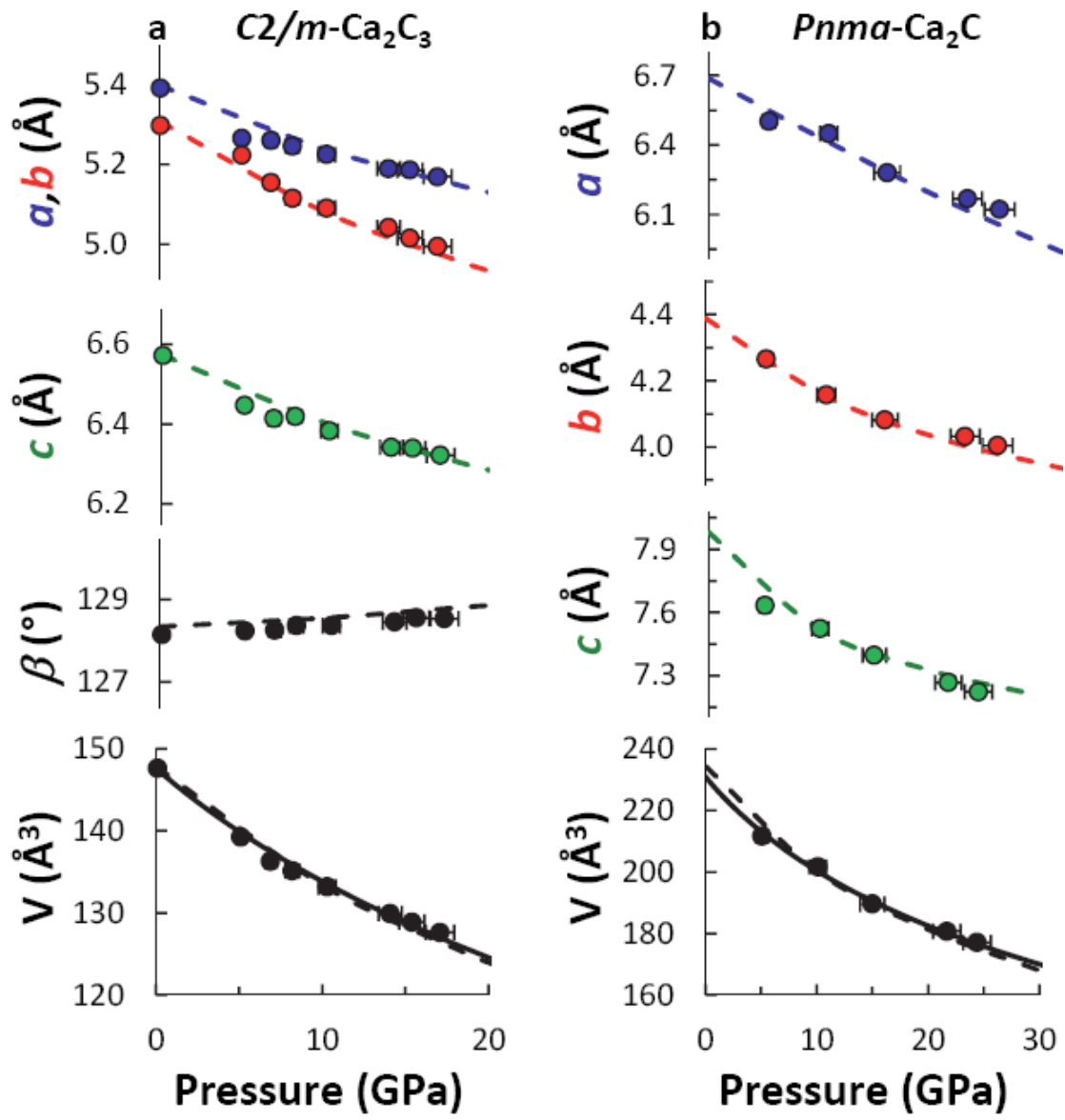
Li *et al.* Fig. 5.



Li *et al.* Fig. 6.



Li *et al.* Fig. 7



Li *et al.* Fig. 8